Journal of Computational Physics 298 (2015) 480–494

Contents lists available at ScienceDirect

Journal of Computational Physics

www.elsevier.com/locate/jcp

# Energy preserving turbulent simulations at a reduced computational cost

F. Capuano [a,b,*], G. Coppola [a], G. Balarac [c], L. de Luca [a]

[a] Dipartimento di Ingegneria Industriale (DII), Università di Napoli "Federico II", Napoli, 80125, Italy
[b] Centro Italiano Ricerche Aerospaziali (CIRA), Capua, 81043, Italy
[c] Grenoble-INP/CNRS/UJF-Grenoble 1, LEGI UMR 5519, Grenoble, F-38041, France

ARTICLE INFO

*Article history:*
Received 1 December 2014
Received in revised form 12 June 2015
Accepted 16 June 2015
Available online 22 June 2015

*Keywords:*
Energy conservation
Computational efficiency
Skew-symmetric form
Runge–Kutta
Turbulent flows

ABSTRACT

Energy-conserving discretizations are widely regarded as a fundamental requirement for high-fidelity simulations of turbulent flows. The skew-symmetric splitting of the nonlinear term is a well-known approach to obtain semi-discrete conservation of energy in the inviscid limit. However, its computation is roughly twice as expensive as that of the divergence or advective forms alone. A novel time-advancement strategy that retains the conservation properties of skew-symmetric-based schemes at a reduced computational cost has been developed. This method is based on properly constructed Runge–Kutta schemes in which a different form (advective or divergence) for the convective term is adopted at each stage. A general framework is presented to derive schemes with prescribed accuracy on both solution and energy conservation. Simulations of homogeneous isotropic turbulence show that the new procedure is effective and can be considerably faster than skew-symmetric-based techniques.

© 2015 Elsevier Inc. All rights reserved.

## 1. Introduction

Demand for accurate numerical computations of turbulent flows, with both DNS and LES, has posed many challenges to the numerical community, pushing research efforts toward the construction of suitable new discretization techniques. In the context of laminar and Reynolds-Averaged Navier–Stokes equations, the classical compromise between accuracy and stability of the discretization has often been represented by upwind-like schemes. This solution, however, has been shown not to be feasible in DNS and LES, owing to the large amount of artificial numerical dissipation introduced by non-centered approximations [1]. On the other hand, the straightforward utilization of central non-dissipative schemes can pose severe stability issues, due to the nonlinear amplification of aliasing errors that occur in computing convective terms [2].

A possible solution to these counteracting requirements lies in the employment of nondissipative discretizations able to mimic, on a discrete level, the conservation of important invariants of the continuous equations [3]. In the context of incompressible flows, discrete conservation of kinetic energy is highly desirable in order to obtain physically relevant solutions [4]. Energy-conserving methods are capable of enforcing a nonlinear stability bound to the discrete solution, allowing for stable long-time integration. Moreover, it is well-known that LES has to be performed with low-dissipation numerical schemes, so that the subgrid-scale model contribution is not overwhelmed by numerical diffusion, and the energy

* Corresponding author.
*E-mail addresses:* f.capuano@cira.it (F. Capuano), gcoppola@unina.it (G. Coppola), guillaume.balarac@legi.grenoble-inp.fr (G. Balarac), deluca@unina.it (L. de Luca).

http://dx.doi.org/10.1016/j.jcp.2015.06.011
0021-9991/© 2015 Elsevier Inc. All rights reserved.

cascade is correctly represented [5]. From a mathematical point of view, conservation of kinetic energy in the inviscid limit can be shown to be strongly related to the preservation of some of the fundamental symmetries of the continuous differential operators on the discrete level [6].

In the framework of spatial discretizations of the convective term, use of the so-called skew-symmetric (or splitting) form, defined as a proper average of divergence and advective forms, has been shown to guarantee *a priori* semi-discrete conservation of energy for several high-order centered schemes, over both regular and staggered grid systems [7]. The skew-symmetric form has also been shown to cause a reduction of aliasing errors with respect to the other formulations [8]. In this regard, spectral simulations of turbulent flows with divergence or advective forms proved to be unstable without dealiasing, while the rotational form gave inaccurate results [9]. For these reasons, the splitting form of the nonlinear convective term has been successfully adopted to yield stable simulations of turbulent flows in the incompressible framework [10,11]. A variable-density version of the skew-symmetric form was first introduced in [12] and recently discussed in [13]. The underlying philosophy has been used to construct robust methods in both finite-difference [14,15] and finite-volume contexts [16,17]. The splitting form is nowadays regularly applied in several highly accurate finite-difference and spectral numerical codes for DNS and LES of turbulent flows [18–20].

However, the major drawback of skew-symmetric-based methods is the increased computational cost with respect to classical divergence or advective forms [21], since evaluation of two derivatives is required for each nonlinear component of the convective term [22]. Any attempt to reduce the number of derivative evaluations in computing the convective term requires the employment of divergence or advective formulations, which are not guaranteed to preserve energy, at least on non-staggered or non-uniform grids. In this context, the request for efficiency suggests the exploration of cheaper alternatives to the skew-symmetric splitting, which are able to retain its favorable conservation and aliasing properties.

In addition to the mentioned issues related to spatial discretization, the time integration procedure also plays a role. In classical analyses, time advancement is performed in a semi-discretized approach, and the conservation properties of the temporal scheme are not usually investigated in detail. Full energy conservation (i.e., in space as well as in time) can only be obtained by means of implicit methods [23], but the strong demand for computational efficiency usually dictates the use of explicit time-stepping algorithms. In summary, the overall discrete energy conservation error typically results in the sum of a spatial and a temporal contribution: the former can be nullified by the use of the skew-symmetric form, the latter by implicit time integration.

In this paper, a novel time-advancement strategy is presented, which generalizes some developments made in a recent paper on scalar nonlinear equations [24]. Here, the underlying philosophy is applied to the more interesting case of turbulent simulations of incompressible Navier–Stokes equations. By weighting temporal and spatial errors, this new method is able to recover the conservation properties of skew-symmetric-based schemes just by using the more economical advective or divergence forms. It has been found that optimal energy-conservation properties can be achieved by properly constructed explicit Runge–Kutta (RK) schemes in which a different form for the convective term is adopted at each stage. The main advantage is that, on equivalent results, this approach is able to halve the CPU time required for the computation of the nonlinear term and, in certain situations, yield a considerable overall time saving for the whole algorithm with respect to skew-symmetric-based techniques.

The paper is organized as follows. In Section 2, the conservation properties of semi-discretized Navier–Stokes equations are reviewed and discussed. The novel 'alternating' strategy is presented in Section 3, while the new Runge–Kutta schemes are derived in Section 4. In Section 5 the results of the numerical tests are reported and analyzed. Concluding remarks are given in Section 6.

## 2. Problem formulation

In this work, the incompressible Navier–Stokes equations

$$\frac{\partial u_i}{\partial t} + \mathcal{N}_i(u) = -\frac{\partial p}{\partial x_i} + \frac{1}{\mathrm{Re}}\frac{\partial^2 u_i}{\partial x_j \partial x_j}, \tag{1}$$

$$\frac{\partial u_i}{\partial x_i} = 0, \tag{2}$$

are considered, where $\mathcal{N}_i(u)$ is the nonlinear convective term and Re is the Reynolds number. The convective term can be cast in several analytically equivalent forms, for instance

$$(Div.)_i \equiv \frac{\partial u_j u_i}{\partial x_j}, \tag{3}$$

$$(Adv.)_i \equiv u_j \frac{\partial u_i}{\partial x_j}, \tag{4}$$

$$(Skew.)_i \equiv \frac{1}{2}\frac{\partial u_j u_i}{\partial x_j} + \frac{1}{2} u_j \frac{\partial u_i}{\partial x_j}. \tag{5}$$

These are referred to as *divergence*, *advective* and *skew-symmetric* forms, respectively. Other forms can also be constructed (e.g., rotational), but will not be considered in this study. When posed on a domain $\Omega$ with periodic boundary conditions,

Eqs. (1)–(2) possess a number of invariants, most notably the momentum $m = \int_\Omega u_i dV$ and, for $\mathrm{Re} \to \infty$, the kinetic energy $e = \int_\Omega u_i^2/2\, dV$, which represent the *linear* and *quadratic* invariants, respectively. In a continuous setting, these properties hold for any expression adopted for the nonlinear term. When discretized, Eqs. (3)–(5) have been shown to behave differently, both in terms of conservation properties [7] and aliasing issues [9]. In the following section, the discrete conservation properties of a class of semi-discretization methods will be analyzed.

### 2.1. Conservation properties of semi-discretized N–S equations

A semi-discretized version of Eqs. (1)–(2) can be expressed as

$$\frac{\mathrm{d}\mathbf{u}}{\mathrm{d}t} + \mathbf{C}(\mathbf{u})\mathbf{u} = -\mathbf{G}\mathbf{p} + \frac{1}{\mathrm{Re}}\mathbf{L}\mathbf{u}, \tag{6}$$

$$\mathbf{M}\mathbf{u} = \mathbf{0}, \tag{7}$$

where $\mathbf{u}$ is the discrete velocity vector containing the three components on the three-dimensional mesh, $\mathbf{u} = \left[\mathbf{u}_x\, \mathbf{u}_y\, \mathbf{u}_z\right]^T$, the matrices $\mathbf{G} \in R^{N_\mathbf{u} \times N_p}$ and $\mathbf{M} \in R^{N_p \times N_\mathbf{u}}$ are the discrete gradient and divergence operators, respectively, while $\mathbf{L} \in R^{N_\mathbf{u} \times N_\mathbf{u}}$ is the block-diagonal Laplacian $\mathrm{diag}(\mathcal{L}, \mathcal{L}, \mathcal{L})$ with $\mathcal{L} \in R^{N_p \times N_p}$. In what follows, it will be assumed that the gradient, divergence and Laplacian operators are discretized consistently, in such a way that the relations $\mathbf{G}^T = -\mathbf{M}$ and $\mathcal{L} = \mathbf{M}\mathbf{G}$ hold. The convective term is expressed as the product of a linear block-diagonal convective operator $\mathbf{C}(\mathbf{u})$ and $\mathbf{u}$:

$$\mathbf{C}(\mathbf{u})\mathbf{u} = \begin{bmatrix} \mathcal{C}(\mathbf{u}) & & \\ & \mathcal{C}(\mathbf{u}) & \\ & & \mathcal{C}(\mathbf{u}) \end{bmatrix} \begin{bmatrix} \mathbf{u}_x \\ \mathbf{u}_y \\ \mathbf{u}_z \end{bmatrix}, \tag{8}$$

in which the operator $\mathbf{C}(\mathbf{u})$ can assume one of the following forms:

$$\mathbf{C}(\mathbf{u}) = \begin{cases} \mathcal{D} \equiv \mathrm{diag}\left(\mathbf{D}_x\mathbf{U}_x + \mathbf{D}_y\mathbf{U}_y + \mathbf{D}_z\mathbf{U}_z\right) & \textit{divergence,} \quad \text{(a)} \\ \mathcal{A} \equiv \mathrm{diag}\left(\mathbf{U}_x\mathbf{D}_x + \mathbf{U}_y\mathbf{D}_y + \mathbf{U}_z\mathbf{D}_z\right) & \textit{advective,} \quad \text{(b)} \\ \mathcal{S} \equiv \frac{1}{2}\left(\mathcal{A} + \mathcal{D}\right) & \textit{skew-symmetric,} \quad \text{(c)} \end{cases} \tag{9}$$

In Eq. (9), the matrices $\mathbf{D}_{(\cdot)}$ and $\mathbf{U}_{(\cdot)}$ represent the discrete derivative operators and the diagonal matrices of the discretized velocity components along the three directions (e.g., $\mathbf{U}_x = \mathrm{diag}(\mathbf{u}_x)$).

A *regular* arrangement of the variables on the grid is employed, for which the velocity components $u_i$ and pressure $p$ are stored at the same points [7]. Centered finite-difference and spectral discretizations on a Cartesian, periodic and equally spaced grid will be considered here. Under such hypotheses, the derivative operators satisfy a discrete summation-by-parts rule; from an algebraic point of view, this implies that the derivative matrices are all skew-symmetric, $\mathbf{D}^T = -\mathbf{D}$. As a consequence, it can easily be shown that the convective operator $\mathcal{S}$ also inherits this property for all $\mathbf{u}$, unlike the other two forms.

The discrete conservation properties can be analyzed by deriving the evolution equation of the discrete kinetic energy $E = \mathbf{u}^T\mathbf{u}/2$, which reads

$$\frac{\mathrm{d}E}{\mathrm{d}t} = -\mathbf{u}^T\mathbf{C}(\mathbf{u})\mathbf{u} - \mathbf{u}^T\mathbf{G}\mathbf{p} + \frac{1}{\mathrm{Re}}\mathbf{u}^T\mathbf{L}\mathbf{u}. \tag{10}$$

In Eq. (10), the pressure term contribution vanishes if $\mathbf{G}^T = -\mathbf{M}$ and $\mathbf{M}\mathbf{u} = 0$. The convective and diffusive terms appear as quadratic forms with associated matrices $\mathbf{C}(\mathbf{u})$ and $\mathbf{L}$, respectively. The diffusive term is clearly not energy-conserving (if properly discretized, the operator $\mathbf{L}$ is a negative-definite matrix), while the convective term conserves energy if the skew-symmetric operator of Eq. (9c) is adopted. In the other two cases, the convection matrices $\mathbf{C}(\mathbf{u})$ are in general not skew-symmetric and hence conservation of energy is not guaranteed.

A more in-depth analysis reveals that errors coming from the divergence and advective forms have opposite signs. The key observation is that, for skew-symmetric discrete derivative operators, the following relation holds

$$\mathcal{A}^T = -\mathcal{D}, \tag{11}$$

which immediately implies $-\mathbf{u}^T\mathcal{A}\mathbf{u} = \mathbf{u}^T\mathcal{D}\mathbf{u}$ and hence that the energy variations due to the divergence and advective forms are equal and of opposite sign.

Adoption of the skew-symmetric splitting, albeit attractive for its beneficial conservation properties, turns out to be more expensive than classical advective and divergence forms. A rough estimate of the computational cost in the two cases shows that the skew-symmetric form requires twice the number of matrix–vector products. The present work aims to develop a new time-advancing strategy that is able to retain the beneficial properties of the skew-symmetric splitting at a reduced computational cost.

## 3. The alternating Runge–Kutta strategy

The rationale underlying this method stems from the fact that the global errors on energy conservation associated with discretized divergence and advective forms have opposite signs. The basic idea is to take advantage of the time-advancement scheme to cancel the errors of these two forms up to a certain order of accuracy. By using only divergence or advective forms, the resulting scheme can be more cost-effective than a skew-symmetric-based one. In the following analysis, only inviscid flow is considered ($\mathrm{Re} \to \infty$), since interest is focused exclusively on the conservation properties of the convective term. The core of the method consists in advancing the governing equations by means of a modified explicit Runge–Kutta algorithm, which can be expressed as

$$\mathbf{u}^{n+1} = \mathbf{u}^n - \Delta t \sum_{i=1}^{s} b_i \mathbf{C}_i(\mathbf{u}_i)\mathbf{u}_i + \Delta t \mathbf{G}\mathbf{p}^{n+1}, \tag{12}$$

$$\mathbf{u}_i = \mathbf{u}^n - \Delta t \sum_{j=1}^{i-1} a_{ij} \left( \mathbf{C}_j(\mathbf{u}_j)\mathbf{u}_j - \mathbf{G}\mathbf{p}_j \right), \tag{13}$$

where $s$ is the number of stages, $a_{ij}$ and $b_i$ are the Runge–Kutta coefficients, and pressure is to be solved from the Poisson equations $\mathbf{p}_j = \mathcal{L}^{-1}\mathbf{M}\mathbf{C}_j(\mathbf{u}_j)\mathbf{u}_j$ and $\mathbf{p}^{n+1} = \mathcal{L}^{-1}\mathbf{M}\sum_{j=1}^{s} b_j \mathbf{C}_j(\mathbf{u}_j)\mathbf{u}_j$. Eqs. (12)–(13) differ from the standard Runge–Kutta procedure in that they can accommodate a different formulation for the nonlinear term within the stages. In fact, the operator $\mathbf{C}$ is indexed by a suffix, meaning that it can be expressed in either divergence or advective form at each stage (Eqs. (9a) and (9b), respectively).

The overall aim of this method is to find a set of coefficients, along with a sequence of divergence and advective forms, that maximizes the formal order of accuracy on solution and energy conservation. A prescribed order of accuracy for the discrete solution $\mathbf{u}$ can be attained by imposing the classical order conditions [25]. The resulting nonlinear system is usually underdetermined: the remaining degrees of freedom can be exploited to impose an additional set of equations for energy conservation. The derivation of these conditions is the central part of the novel procedure and will be described in the next section.

### 3.1. Energy analysis

The total energy error introduced over a single time step advancement by Eqs. (12)–(13) can be obtained by taking the inner product between $\mathbf{u}^{n+1}$ and itself. By defining $\Delta E = E^{n+1} - E^n$, Eqs. (12)–(13) can be manipulated to yield

$$\frac{\Delta E}{\Delta t} = \underbrace{-\sum_{i=1}^{s} b_i \mathbf{u}_i^T \widetilde{\mathbf{C}}_i(\mathbf{u}_i)\mathbf{u}_i}_{I} \underbrace{- \frac{\Delta t}{2} \sum_{i,j=1}^{s} \left( b_i a_{ij} + b_j a_{ji} - b_i b_j \right) \mathbf{u}_i^T \widetilde{\mathbf{C}}_i^T(\mathbf{u}_i) \widetilde{\mathbf{C}}_j(\mathbf{u}_j)\mathbf{u}_j}_{II}, \tag{14}$$

where the matrices $\widetilde{\mathbf{C}}_i$ are the discrete convective operators projected with the pressure gradient to yield a divergence free velocity field, i.e. $\widetilde{\mathbf{C}}_i = \mathbf{P}\mathbf{C}_i$, where $\mathbf{P} = \mathbf{I} - \mathbf{G}\mathcal{L}^{-1}\mathbf{M}$. The two terms on the right-hand side of Eq. (14) can be defined as

I) *Spatial* error: $\sum_{i=1}^{s} b_i \mathbf{u}_i^T \widetilde{\mathbf{C}}_i(\mathbf{u}_i)\mathbf{u}_i$,

II) *Temporal* error: $\frac{\Delta t}{2} \sum_{i,j=1}^{s} \left( b_i a_{ij} + b_j a_{ji} - b_i b_j \right) \mathbf{u}_i^T \widetilde{\mathbf{C}}_i^T(\mathbf{u}_i) \widetilde{\mathbf{C}}_j(\mathbf{u}_j)\mathbf{u}_j$.

The first depends primarily on spatial discretization, as the $s$ quadratic forms are identically zero if skew-symmetric matrices $\widetilde{\mathbf{C}}_i$ are adopted. The second quantity has a more complex structure, and can be nullified by so-called symplectic methods [23], a special class of implicit Runge–Kutta schemes for which $b_i a_{ij} + b_j a_{ji} - b_i b_j = 0$. For standard methods ($\widetilde{\mathbf{C}}_i \equiv \widetilde{\mathbf{C}}$), the temporal error inherits the same order of the scheme and does not vanish in general, even in the case of skew-symmetric operators $\widetilde{\mathbf{C}}$.

The use of different discretized forms inside the stages of the Runge–Kutta procedure gives rise to new possibilities for obtaining cost-effective energy-preserving algorithms. An appropriate choice of Runge–Kutta coefficients can lead to methods in which the mixed spatial and temporal errors are nullified up to a certain order of accuracy.

The starting point of the analysis is the expansion of Eq. (14) as a Taylor series in the time increment $\Delta t$. To this end, Eqs. (12)–(13) can be plugged into Eq. (14); by using the linearity of the convective operator $\widetilde{\mathbf{C}}_i(\mathbf{u}_i)$ with respect to $\mathbf{u}_i$, after some manipulation one obtains (cf. [24])

$$\frac{\Delta E}{\Delta t} = \overbrace{-\mathbf{u}^T \left[ \sum_i b_i \widetilde{\mathbf{C}}_i \right] \mathbf{u}}^{1^{\text{st}}\text{ order term}} + \underbrace{\frac{\Delta t}{2} \mathbf{u}^T \left[ \sum_{ij} 2 b_i a_{ij} \left( \widetilde{\mathbf{C}}_i \widetilde{\mathbf{C}}_j + \widetilde{\mathbf{C}}_{ij} \right) + g_{ij} \widetilde{\mathbf{C}}_i^T \widetilde{\mathbf{C}}_j \right] \mathbf{u}}_{2^{\text{nd}}\text{ order term}} + O\left( \Delta t^2 \right), \tag{15}$$

where $\mathbf{u} = \mathbf{u}^n$, $g_{ij} = b_i a_{ij} + b_j a_{ji} - b_i b_j$, $\widetilde{\mathbf{C}}_{ij} = \widetilde{\mathbf{C}}_i\left(\widetilde{\mathbf{C}}_j\left(\mathbf{u}^n\right)\mathbf{u}^n\right)$, with parentheses denoting functional dependence. In Eq. (15) and hereinafter, the operator $\mathbf{C}$ is assumed to be evaluated at $\mathbf{u}^n$ if not otherwise specified.

Equation (15) constitutes the basic relation for construction of optimized Runge–Kutta schemes. A proper choice of the coefficients $b_i$ and $a_{ij}$ can nullify both the first- and second-order terms appearing in Eq. (15), leading to schemes with optimal conservation properties. Determination of a suitable set of conditions is obtained in four steps:

($a$) fix the number of stages of the method;
($b$) choose a sequence of advective (A) and divergence (D) forms;
($c$) group the resulting terms of Eq. (15) into combinations of few independent terms;
($d$) impose conditions on $a_{ij}$ and $b_i$ to nullify the terms.

As regards step ($c$), it is easy to show that Eq. (11) allows the various products or compositions of matrices $\widetilde{\mathbf{C}}_i$ to be transformed into groups of fewer independent terms. In particular, the linear combination appearing in the first-order contribution can be collected into a single term proportional to a quadratic form in which only one of the two operators $\widetilde{\mathcal{D}}$ or $\widetilde{\mathcal{A}}$ is present (the projection operator is easily seen to be irrelevant in this term, provided that $\mathbf{Mu} = 0$). By employing Eq. (11), and after some manipulation, it can also be shown that each of the $3s$ terms $\widetilde{\mathbf{C}}_i\widetilde{\mathbf{C}}_j$, $\widetilde{\mathbf{C}}_i(\widetilde{\mathbf{C}}_j\mathbf{u})$ and $\widetilde{\mathbf{C}}_i^T\widetilde{\mathbf{C}}_j$ can be substituted, inside the quadratic form, by one of the three basic forms $\widetilde{\mathcal{A}}\widetilde{\mathcal{A}}$, $\widetilde{\mathcal{A}}\widetilde{\mathcal{D}}$, and $\widetilde{\mathcal{D}}\widetilde{\mathcal{A}}$. For a detailed description of this procedure in a one-dimensional setting the reader is referred to [24]. Note that in that case the analysis is conducted by employing, in place of Eq. (11), the relation $\mathcal{A}^T = -2\mathcal{D}$, which is the corresponding relation between advective and divergence operators in the one-dimensional formulation. A similar analysis performed on the basis of Eq. (11) easily leads to the relations

$$\widetilde{\mathcal{A}}\left(\widetilde{\mathcal{A}}\mathbf{u}\right) \sim -\widetilde{\mathcal{D}}\widetilde{\mathcal{A}}, \tag{16}$$

$$\widetilde{\mathcal{A}}\left(\widetilde{\mathcal{D}}\mathbf{u}\right) \sim -\widetilde{\mathcal{D}}\widetilde{\mathcal{D}}, \tag{17}$$

$$\widetilde{\mathcal{D}}\left(\widetilde{\mathcal{A}}\mathbf{u}\right) \sim \widetilde{\mathcal{D}}\widetilde{\mathcal{A}}, \tag{18}$$

$$\widetilde{\mathcal{D}}\left(\widetilde{\mathcal{D}}\mathbf{u}\right) \sim \widetilde{\mathcal{D}}\widetilde{\mathcal{D}}, \tag{19}$$

where parentheses denote functional dependence. The equivalence relation $\sim$ applies to matrix operators and holds when the corresponding quadratic forms associated with a vector $\mathbf{u}$ are equal for any value of $\mathbf{u}$, e.g.

$$\mathcal{A}\left(\mathcal{A}\mathbf{u}\right) \sim -\mathcal{D}\mathcal{A} \qquad \Longleftrightarrow \qquad \mathbf{u}^T\mathcal{A}\left(\mathcal{A}\mathbf{u}\right)\mathbf{u} = -\mathbf{u}^T\mathcal{D}\mathcal{A}\mathbf{u} \quad \forall\,\mathbf{u} \in R^{N_\mathbf{u}}. \tag{20}$$

The presence of the projection operator, which is peculiar to Navier–Stokes discretizations, does not influence the equivalence relation between the various operators inside the quadratic forms, provided that the velocity fields involved are divergence free, i.e. $\mathbf{Pu} = \mathbf{u}$. The application of step ($d$) leads to the conclusion that one additional linear constraint on the coefficients $b_i$ has to be added to enforce first-order conservation of energy, whereas three nonlinear equations on the coefficients $b_i$ and $a_{ij}$ are needed for second-order conservation. The constraints on energy can be coupled to classical order conditions to give a global system for determining new Runge–Kutta schemes.

## 4. New Runge–Kutta schemes

In principle, alternating Runge–Kutta schemes with an arbitrary number of stages can be derived and analyzed. Here, attention will be focused on three- and four-stage methods, which allow for a relatively large number of degrees of freedom and have been applied historically to numerical simulations of turbulent flows.

An $s$-stage RK method gives $s(s+1)/2$ degrees of freedom. Second-, third- and fourth-order conditions on the solution take 2, 4 and 8 equations, respectively, whereas the first- and second-order conditions on energy conservation for alternating schemes take 1 and 3 equations. Depending on the number of available parameters provided by the method, order conditions and energy-preserving properties can be combined in many different ways to obtain several families of schemes. In order to handle all possibilities, the new classes of methods are labeled by an acronym indicating the order of accuracy on solution (S) and on energy conservation (E). A cost-coefficient proportional to the number of derivatives required per time step is also reported in brackets, to serve as a simple cost metric for comparing the performances of the various schemes. In general, the number of matrix–vector products is reasonably approximated by $sd^2$ for advective and divergence forms and $2sd^2$ for the skew-symmetric form, where $d$ is the number of dimensions. For simplicity, $d = 1$ will be assumed hereinafter for the estimation of the cost-coefficients. In this simplified metric, the cost of the skew-symmetric splitting is doubled with respect to divergence and advective forms. The results of a more detailed cost analysis show that this is in many cases a very good approximation, at least for explicit finite-difference schemes [24].

In order to keep the presentation as clear as possible, only the Butcher arrays of the new schemes will be given here. Details about the nonlinear systems and their general solutions are reported in Appendix A.

### 4.1. Three-stage methods

Explicit three-stage methods provide 6 degrees of freedom. As a consequence, two families of new schemes should be expected: 2S2E(3) (6 conditions) and 3S1E(3) (5 conditions), for a total number of $2^s - 2$ possible sequences of advective and divergence forms (the sequences constructed uniquely by one form are excluded). In the following, each sequence will be indicated by a string composed by the letters A or D, to denote the use of the advective or divergence form, respectively. For instance, the sequence ADA means that the advective form is used in the first and third stages, while for the second stage the divergence form is adopted.

As regards 2S2E(3) schemes, no solutions were found, for any of the 6 sequences available. This result is in contrast with the one-dimensional case, where plenty of results are obtainable [24].

On the other hand, the derivation of 3S1E(3) schemes is straightforward and can be achieved by imposing the order-1 condition on energy conservation on the parametrized families given in [25]. For instance, the "case II" and "case III" one-parameter families of schemes reported in [25]:

case II

$$\begin{array}{c|ccc} 0 & & & \\ \frac{2}{3} & 0 & & \\ \frac{2}{3} - \frac{1}{4b_3} & \frac{1}{4b_3} & 0 & \\ \hline & \frac{1}{4} & \frac{3}{4} - b_3 & b_3 \end{array}$$

case III

$$\begin{array}{c|ccc} 0 & & & \\ \frac{2}{3} & 0 & & \\ -\frac{1}{4b_3} & \frac{1}{4b_3} & 0 & \\ \hline & \frac{1}{4} - b_3 & \frac{3}{4} & b_3 \end{array},$$

generate 3S1E(3) schemes when the free parameter is fixed in such a way that the linear constraint on 1st-order energy conservation is enforced for each sequence of divergence and advective forms. The results of this analysis are that "case II" schemes obtained with $b_3 = 1/4$ or $b_3 = 1/2$ ensure first order conservation of energy when employed with the sequences DAD (or ADA) and DDA (or AAD), respectively. The "case III" schemes corresponding to $b_3 = -1/4$ or $b_3 = 1/2$, on the other hand, are 3S1E(3) schemes when employed with the sequences ADD (or DAA) and DDA (or AAD), respectively. These latter schemes possess negative $b_i$ coefficients. This is not desirable in Runge–Kutta methods for stability reasons [25], hence the two schemes derived from "case II" are to be preferred.

### 4.2. Four-stage methods

In four-stage methods, 10 degrees of freedom are available. Hence, either 4S1E(4) or 3S2E(4) schemes can be constructed, which have to be compared to 4S4E(8) skew-symmetric methods.

A large number of 4S1E(4) schemes can easily be obtained by applying the first-order condition on energy to the parametrized fourth-order families provided in classical books (e.g., [25]). Perhaps the most convenient choice is to use an alternating version of the classical Runge–Kutta scheme (RK4), as it can be conveniently implemented. If one employs an ADAD or a DADA sequence inside the stages, the RK4 satisfies the first-order condition on energy conservation while retaining fourth-order accuracy on solution,

ADAD/DADA − 4S1E(4)

$$\begin{array}{c|cccc} 0 & & & & \\ \frac{1}{2} & 0 & & & \\ 0 & \frac{1}{2} & 0 & & \\ 0 & 0 & 1 & 0 & \\ \hline & \frac{1}{6} & \frac{1}{3} & \frac{1}{3} & \frac{1}{6} \end{array}.$$

The alternating RK4 will be considered as the reference 4S1E(4) scheme for the subsequent sections.

In the case of 3S2E(4) schemes, solutions exist only for the two couples of sequences ADAD/DADA and ADDA/DAAD. For details on the nonlinear systems, the reader is referred to Appendix A. Here, two Butcher arrays will be given which are particularly compact

ADAD/DADA − 3S2E(4)

$$\begin{array}{c|cccc} 0 & & & & \\ \frac{1}{2} & 0 & & & \\ \frac{5}{12} & \frac{5}{12} & 0 & & \\ 0 & \frac{5}{14} & \frac{1}{7} & 0 & \\ \hline & \frac{1}{5} & \frac{3}{20} & \frac{3}{10} & \frac{7}{20} \end{array}$$

ADDA/DAAD − 3S2E(4)

$$\begin{array}{c|cccc} 0 & & & & \\ \frac{1}{3} & 0 & & & \\ 0 & 1 & 0 & & \\ \frac{1}{3} & 0 & \frac{1}{3} & 0 & \\ \hline & \frac{1}{8} & \frac{3}{8} & \frac{1}{8} & \frac{3}{8} \end{array},$$

having both third-order accuracy on the solution and second-order accuracy on energy conservation. In Appendix B, it is shown that the two-parameter family of schemes for the sequences ADAD/DADA has the absolute stability footprint of a three-stage scheme. On the contrary, the ADDA/DAAD scheme is fourth-order accurate for linear equations. Therefore, the latter will be the reference 3S2E(4) scheme for the numerical tests presented in the following section.

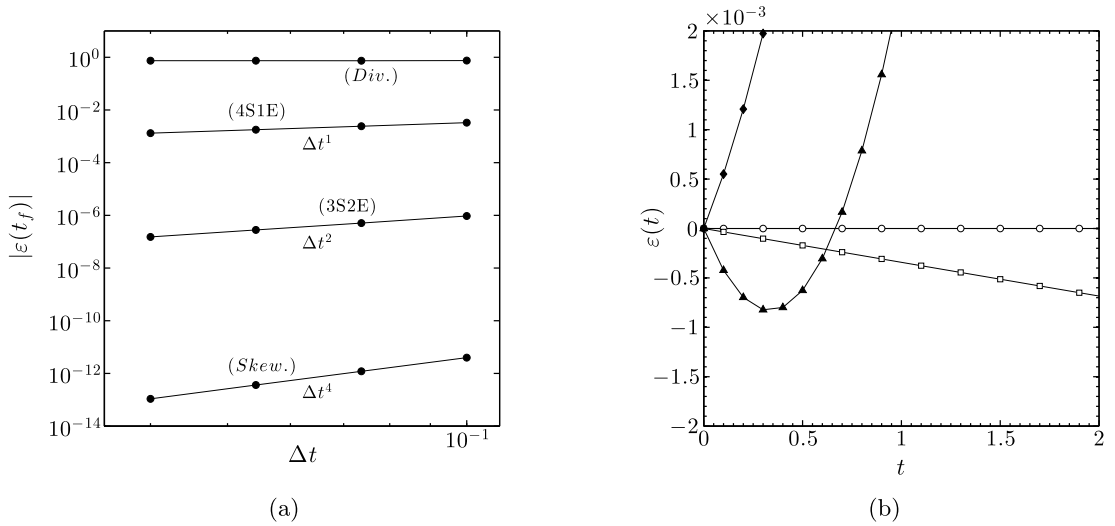


**Fig. 1.** Results for 2D periodic, inviscid flow simulations. (a) Time-step convergence of the relative error on energy conservation. (b) Time evolution of kinetic energy conservation error; — (*Skew.*), ▲ (*Adv.*), ♦ (*Div.*), □ (4S1E), ○ (3S2E). All simulations performed with $\Delta t = 0.1$.

## 5. Numerical results

In this section, the alternating strategy is applied to a number of numerical tests. The aim of the analysis is twofold: to prove the consistency of the theoretical framework and to assess the performances of the new schemes. To pursue these scopes, an order of accuracy analysis is first performed; then, the novel methods are systematically compared to a reference 4S4E(8) solution obtained by using the skew-symmetric form in conjunction with the classical RK4 scheme. Two different solution algorithms will be considered in this study: a finite-difference method (in physical space) and a pseudo-spectral method (in wavenumber space). The final goal is to show that the optimized schemes give similar results to the reference one at a reduced computational cost, in benchmark cases as well as in more realistic situations.

Five methods will be considered; they are listed as follows, along with a short string that will be used to indicate them hereinafter:

- nonlinear term discretized in skew-symmetric form in conjunction with RK4, (*Skew.*);
- nonlinear term discretized in advective form in conjunction with RK4, (*Adv.*);
- nonlinear term discretized in divergence form in conjunction with RK4, (*Div.*);
- alternating DAAD − 3S2E(4) scheme, (3S2E);
- alternating DADA − 4S1E(4) scheme, (4S1E).

It is worth noting that the resulting linear stability region is, in all cases, that of a four-stage, fourth-order Runge–Kutta scheme. Hence, the maximum CFL allowed by discretization of convection is $\approx 0.907$ for a fully spectral accuracy and $\approx 2.85$ for a second-order finite-difference scheme [26].

### 5.1. Order of accuracy study

Two-dimensional, inviscid flow simulations are carried out on a periodic domain to confirm the theoretical results obtained in the previous sections. To this aim, following [7], a square region of size $2\pi L \times 2\pi L$ is considered, discretized on a mesh of $16 \times 16$ mesh points. The solenoidal initial velocity field is constructed from a stream function of random numbers, normalized such that $\mathbf{1}^T \mathbf{u}_x = \mathbf{1}^T \mathbf{u}_y = 0$ and $E_0 = 1.0$, where $\mathbf{1}$ is the column vector of all ones (discrete integrator on uniform mesh) and $E_0 = E(t = 0)$. A random initial condition guarantees that the flowfield is devoid of any symmetries, and hence prevents any apparent order improvement. A centered second-order finite-difference scheme is used for convection; for time-advancement, the various Runge–Kutta schemes developed in Section 4 are used.

The following error measure is defined

$$\varepsilon(t) = \frac{E(t) - E_0}{E_0}, \tag{21}$$

which represents the relative error on kinetic energy conservation at each time instant $t$.

Fig. 1(a) shows the time step convergence of the energy error for four Runge–Kutta methods. The convergence is measured at $t = t_f = 10$, where time is expressed in units of $L/\sqrt{E_0}$, as in [7]. The slopes confirm the predicted orders of

**Table 1**
Results for 2D periodic, inviscid flow simulations. Kinetic energy conservation errors at $t = 2$ and $t = t_f = 10$ (see Fig. 1) for different Runge–Kutta methods and convective forms.

| Scheme | $\varepsilon(t=2)$ | $\varepsilon(t=10)$ |
|---|---|---|
| (*Div.*) | 0.0315 | 0.7503 |
| (*Adv.*) | 0.0200 | 0.8404 |
| (*Skew.*) | $1.3420 \times 10^{-12}$ | $3.9737 \times 10^{-12}$ |
| (3S2E) | $-4.9925 \times 10^{-8}$ | $-9.4583 \times 10^{-7}$ |
| (4S1E) | $-6.8404 \times 10^{-4}$ | $-3.2929 \times 10^{-3}$ |

accuracy for the new schemes (4S1E) and (3S2E), proving the consistency of the theoretical framework. The divergence form gives a constant error, which corresponds to the spatial contribution of Eq. (14); a similar behavior is found for the advective form (not shown here). The first part of the time-evolution of the energy error is shown in Fig. 1(b). The non-conservative formulations show a large error growing steeply during the first instants of the simulation. On the contrary, the (*Skew.*) method as well as the alternating Runge–Kutta schemes remain bounded; in particular, the (3S2E) scheme is identical to the skew-symmetric method within the plotting accuracy. It is interesting to observe that, in the very first part of the simulation, the (*Div.*) and (*Adv.*) methods provide errors which are approximately equal and of opposite sign, as predicted by Eq. (11), that is a linear approximation. Then, nonlinearity takes place and the violation in energy conservation leads to a sudden blow-up.

Table 1 gives a more detailed comparison among the errors provided by the various methods. It is worth noting that the novel methods are dissipative, hence the simulation is stable for long-time integration.

### 5.2. Finite-difference simulation of temporal mixing layer

As a second test case, a temporal mixing layer is considered, which is a well-known benchmark to study the properties of a numerical algorithm in terms of handling steep gradients and formation of smaller scales. The domain is a square region of size $2\pi \times 2\pi$ with periodic boundary conditions. A very coarse mesh of $20^2$ points is used to prove the robustness of the various schemes. Simulations are carried out with a constant time step $\Delta t = 10^{-2}$ and no viscosity. The algorithm adopted for this test is a second-order finite-difference code. The Poisson equation for pressure is solved in physical space after each Runge–Kutta sub-step using an unpreconditioned Bi-CGStab iterative method [27]. The initial flowfield is given by

$$u = \begin{cases} \tanh\left(\frac{y-\pi/2}{\delta}\right), & y \le \pi, \\ \tanh\left(\frac{3\pi/2-y}{\delta}\right), & y > \pi, \end{cases} \tag{22}$$

$$v = \epsilon \sin(x), \tag{23}$$

and is actually a double mixing layer to allow for the use of periodic boundary conditions. The perturbation on the $v$-velocity is used to promote the roll-up of the shear layer; as in [23], $\epsilon = 0.05$ is used. A single instability mode is activated by choosing $\delta = \pi/15$ [28].

In Fig. 2, the iso-contours of the vorticity field at $t = 8$ are shown for four methods. The (*Skew.*) contour is identical to the ones resulting from (4S1E) and (3S2E) methods. While for this test the divergence form blew-up due to over-production of energy, the advective form dissipates the kinetic energy of the flow, and the resulting vorticity field is much more smeared in comparison to the conservative formulations. Further insight is given by observing the time-evolution of the energy error $|\varepsilon(t)|$ as well as the two-dimensional energy spectra calculated at $t = 8$, both shown in Fig. 3. The advective form provides a large amount of dissipation, especially at the highest wavenumbers. The alternating schemes perform remarkably well, particularly the (3S2E). In Fig. 3(b), the curves of the methods (4S1E), (3S2E) and (*Skew.*) are coincident.

Measurements of the CPU time spent for the computation of the nonlinear term have confirmed the doubled cost of the skew-symmetric splitting with respect to the other formulations. For what concerns the entire solution algorithm, most of the time is clearly spent by the Poisson solver. In the present implementation, enforcing mass conservation at each RK sub-step took the 80% of the total time, on average. As a consequence, the novel schemes allowed an overall time saving of about 7% with respect to the skew-symmetric form, although these data are strongly dependent upon a large number of factors, including computational and programming issues. The cost of the projection step could be reduced by enforcing mass conservation only at the final RK stage, as in [29].

### 5.3. Spectral simulations of Homogeneous Isotropic Turbulence (HIT)

In this section, simulations of homogeneous isotropic turbulence (HIT) are performed. A standard pseudo-spectral code has been adopted here, using a projection method in spectral space to enforce the divergence-free condition. The pseudo-spectral solver uses a classical parallel design based on two-dimensional subdivisions. The 3D Fast Fourier Transform (FFT) is split in three one-dimensional transforms. The parallelization is carried out by subdividing the 3D geometry along only 2 directions: along Y and Z in the real space and along X and Y on the spectral space. The code has been recently used to

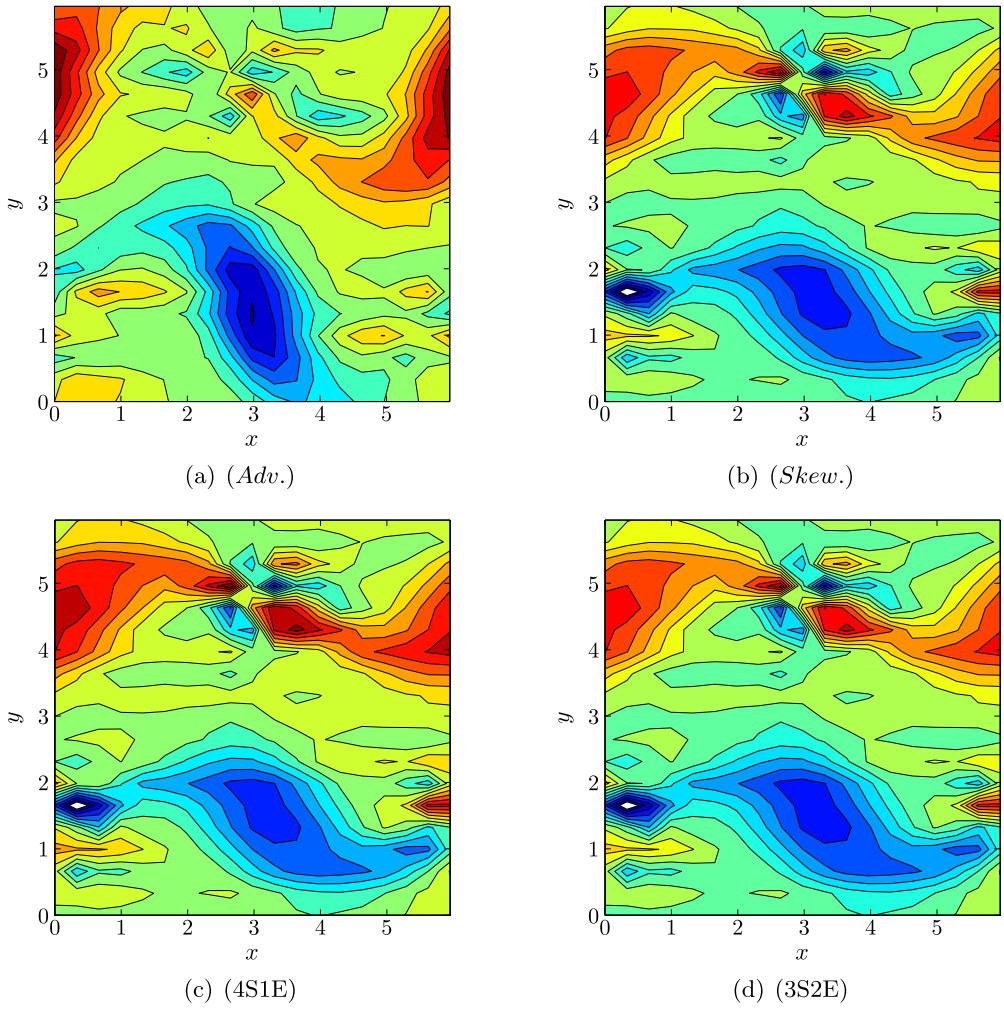


**Fig. 2.** Vorticity contours of mixing layer at $t = 8$. Iso-contours ranging from $-4$ to 4 with steps 0.5.

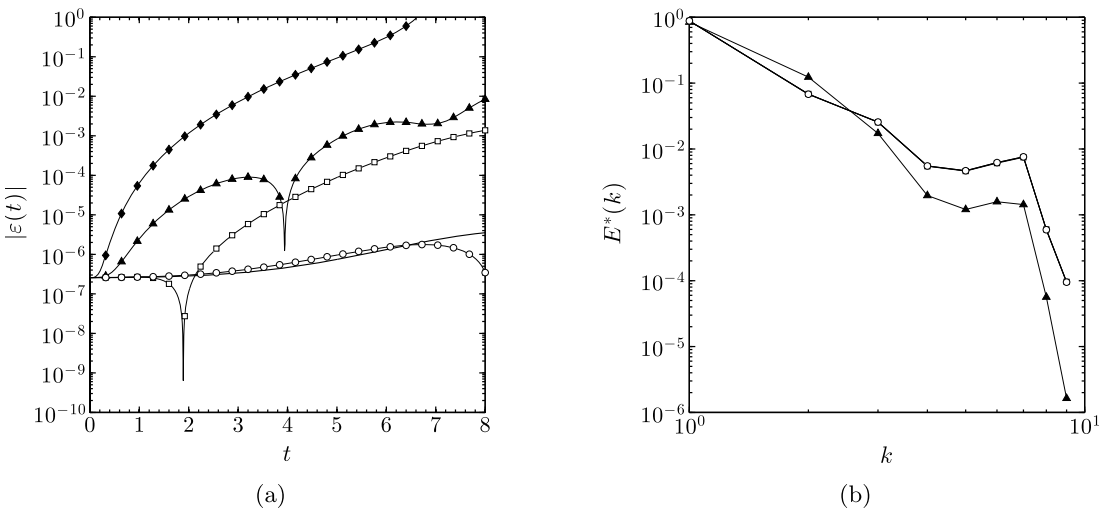


**Fig. 3.** Results for the mixing layer; — (*Skew.*), ▲ (*Adv.*), ♦ (*Div.*), □ (4S1E), ○ (3S2E). (a) Time-evolution of kinetic energy conservation error. (b) Two-dimensional energy spectra at $t = 8$. Energy is normalized by its initial value.

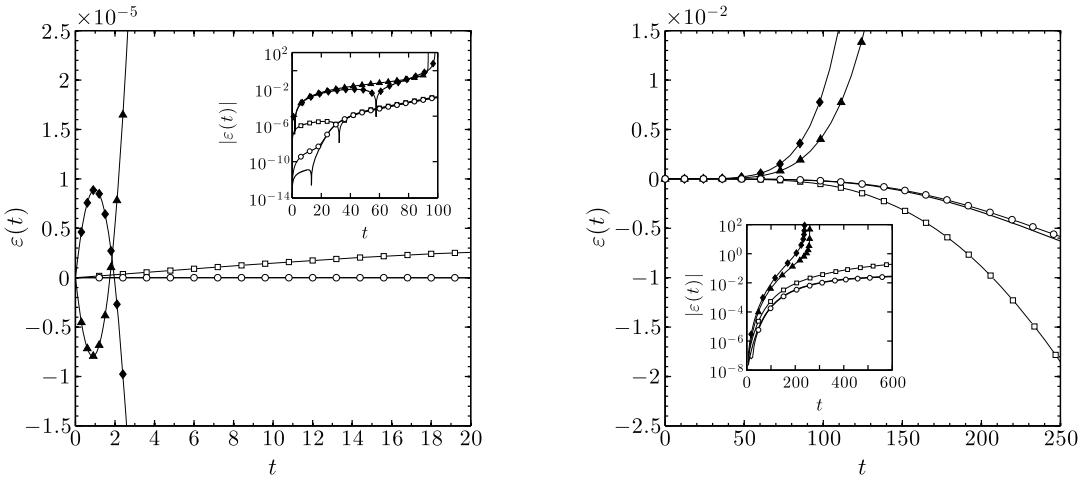


**Fig. 4.** Time evolution of the energy-conservation error for inviscid HIT, for two spatial discretizations. The inset plots show the absolute value of the error in logarithmic scale at longer times. — (*Skew.*), ▲ (*Adv.*), ♦ (*Div.*), □ (4S1E), ○ (3S2E).

test a hybrid spectral-particle method for the turbulent transport of a passive scalar [30]. All derivatives are performed in spectral space and all products are performed in physical space.

*5.3.1. Inviscid HIT*

At first, an inviscid case is considered. This kind of test proved to be useful to assess the robustness of numerical algorithms in both incompressible and compressible frameworks [14]. Simulations are carried out on a coarse grid of $32^3$ points, on a domain of length $2\pi$. The initial condition is designed to satisfy a given energy spectrum, typical of decaying isotropic turbulence. The aim of the test is mainly to prove that the novel alternating procedure retains the energy-conservation properties of the reference skew-symmetric method also in situations characterized by a multi-scale initial flowfield. A fully spectral and a second-order finite-difference scheme are considered, the latter being emulated by means of the modified wavenumber approach [9]. The tests are performed without subgrid-scale (SGS) model and the simulations are not de-aliased. The various cases differ only by the form of the convective term and the Runge–Kutta scheme used for time advancement.

Fig. 4 shows the time-evolution of the kinetic energy error $\varepsilon(t)$ for both the second-order and the spectral scheme. The linear-scale graphs focus on the early instants of the simulations, while the inset plots in logarithmic scale provide a comparison for long-time integration in terms of the absolute value of the error. For both the spatial discretization schemes considered, the advective and divergence forms diverge due to violation of kinetic energy conservation. On the other hand, the energy-preserving formulations are stable. In particular, the (3S2E) scheme is very close to the (*Skew.*) method, while the (4S1E) shows some deviation, which is particularly evident for the spectral case. Also, in the spectral simulations the non-conservative forms take longer times to develop the nonlinear instability. Recall that the error $\varepsilon(t)$ for the (*Skew.*) method is due solely to the RK4 used for time integration (i.e., the *temporal* error), while for the alternating schemes it is a mix of spatial and temporal errors. The outcome of the comparison is positive because the alternating procedure mimics the results of the skew-symmetric splitting.

These considerations are confirmed by the numerical results shown in Table 2. The relative energy error $\varepsilon(t)$ is reported for both the second-order and the spectral accuracy; the times are chosen in order to show the numerical errors before and after the blow-up of the divergence and advective formulations. The errors provided by the alternating schemes and by the skew-symmetric form are dissipative. As a consequence, for such methods the discretization of the convective term does not spuriously produce kinetic energy, and the simulation is stable. As in Fig. 1(b), the (*Adv.*) and (*Div.*) errors shown in Fig. 4(a) are approximately equal and of opposite sign in the first instants of the simulation.

*5.3.2. Forced HIT*

As a final test, direct and large-eddy simulations of forced HIT are performed. The forcing strategy consists in *freezing* the low wavenumbers ($|\vec{k}| \leq 2$), to avoid the introduction of randomness as in classic forcing schemes [31]. The convective term is discretized with full spectral accuracy, while the diffusive term is computed exactly, thus without introducing any viscous time step restriction. Two Reynolds numbers (based on the Taylor micro-scale $\lambda$) are considered: $\mathrm{Re}_\lambda = 100$ and $\mathrm{Re}_\lambda = 170$. The time step is computed from the CFL condition imposed by the convective term, with a maximum CFL number of 0.5. All the results shown here correspond to no-dealiased simulations.

For DNS, the Navier–Stokes equations are discretized using $256^3$ grid points on a domain of length $2\pi$. Fig. 5 shows the kinetic energy evolution in time and the three-dimensional energy spectra for various Runge–Kutta schemes and convective

**Table 2**
Kinetic energy conservation errors (see Fig. 4) for different methods and spatial discretizations.

| Scheme | Second-order | | Spectral | |
|---|---|---|---|---|
| | $\varepsilon(t=40)$ | $\varepsilon(t=100)$ | $\varepsilon(t=100)$ | $\varepsilon(t=300)$ |
| (*Div.*) | $-8.925\times10^{-3}$ | $+\infty$ *(blow-up)* | $7.772\times10^{-3}$ | $+\infty$ *(blow-up)* |
| (*Adv.*) | $1.806\times10^{-2}$ | $+\infty$ *(blow-up)* | $4.016\times10^{-3}$ | $+\infty$ *(blow-up)* |
| (*Skew.*) | $-9.571\times10^{-6}$ | $-1.157\times10^{-3}$ | $-2.006\times10^{-4}$ | $-9.792\times10^{-3}$ |
| (3S2E) | $-9.578\times10^{-6}$ | $-1.157\times10^{-3}$ | $-1.793\times10^{-3}$ | $-9.111\times10^{-3}$ |
| (4S1E) | $-9.552\times10^{-6}$ | $-1.393\times10^{-3}$ | $-5.192\times10^{-3}$ | $-3.251\times10^{-2}$ |

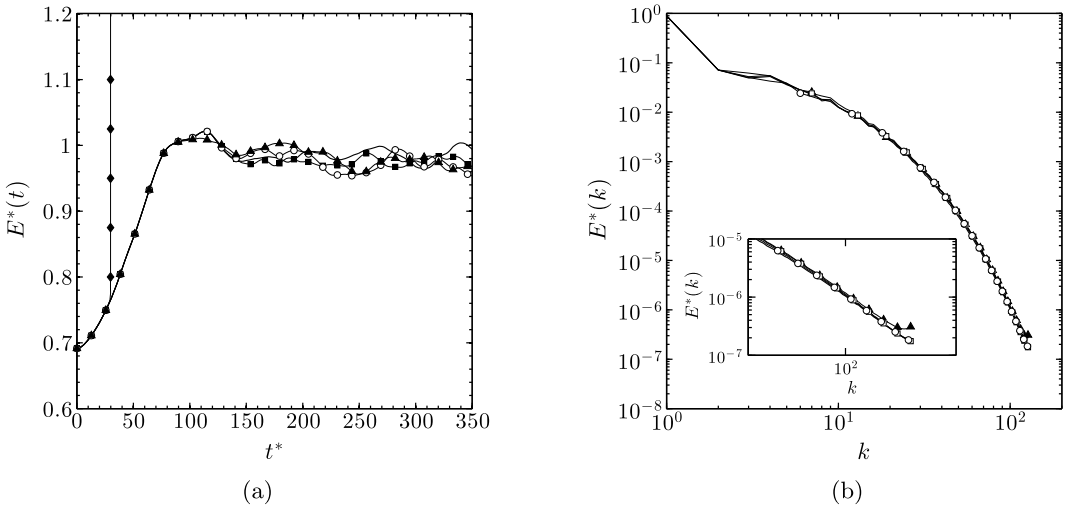


**Fig. 5.** Results for direct numerical simulation of forced HIT for $\mathrm{Re}_\lambda = 170$; — (*Skew.*), ▲ (*Adv.*), ♦ (*Div.*), □ (4S1E), ○ (3S2E). (a) Time evolution of kinetic energy normalized by the steady-state value. Time is expressed in a viscous scale. (b) Three-dimensional energy spectra at $t^* = 720$. Energy is normalized by the steady-state value. The inset plot shows a close-up of the tail of the spectrum.

forms, for $\mathrm{Re}_\lambda = 170$. The divergence form is unstable, while all the other methods are found to be stable. However, an analysis in spectral space reveals that the advective form exhibits a deviation from the other curves at the highest wavenumbers, that is caused by violation of energy conservation and is best revealed by the close-up of Fig. 5(b).

In this test, the projection method does not require any costly Poisson solver, hence the computation of the convective term has an important impact on the global computational time. The proposed Runge–Kutta schemes allowed a global saving in CPU time of about 43% with respect to the skew-symmetric form. This important time-saving was measured for a single time step and is independent of the mesh-size. In the spectral algorithm used in this work, it is due to the fact that the skew-symmetric form needs roughly to perform twice as many forward and inverse FFTs for each sub-step of the Runge–Kutta scheme as those required by divergence or advective forms alone.

In large-eddy simulations, a dynamic Smagorinsky model is used to account for subgrid-scales [32,33]. The computational grid consists of $64^3$ points. The results for $\mathrm{Re}_\lambda = 100$ are shown in Fig. 6. Apparently, none of the methods undergo a nonlinear instability in the time intervals considered. However, the spectral analysis shows that the divergence and advective forms exhibit a significant pile-up at high wavenumbers, while the results provided by the alternating methods are very similar to those obtained using the skew-symmetric form. This proves that the beneficial aliasing properties of the skew-symmetric form are also retained by the new schemes. For each graph, the corresponding DNS curve computed with the skew-symmetric splitting is also shown for comparison, and the agreement with LES is overall satisfactory.

In the case of $\mathrm{Re}_\lambda = 170$, shown in Fig. 7, these effects are even more pronounced. In fact, as the Reynolds number grows, the flowfield gets increasingly under-resolved and the effects of non-conservation of discrete energy are enhanced.

Note that for LES, the skew-symmetric form adds only 15% of additional CPU time, because the SGS model computation with the dynamic procedure has a significant impact on the overall CPU time. It is known that the use of an SGS model written in physical space is computationally expensive, especially when a dynamic procedure is used to evaluate the model coefficient. In fact, a pseudo-spectral code needs to compute various forward and inverse FFTs to apply the model. The SGS model contribution to the overall computational cost could be reduced by using spectral SGS models.

## 6. Conclusions

A novel time-advancing strategy has been developed for efficient energy preserving simulations of incompressible turbulent flows. The method is based on a Runge–Kutta scheme in which the divergence or advective forms for convection

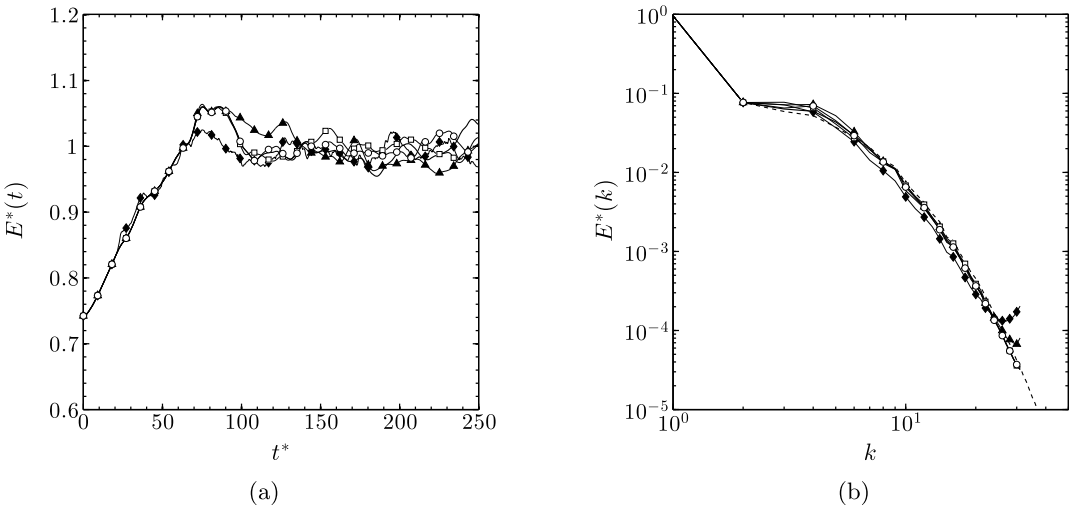


**Fig. 6.** Results for large-eddy simulation of forced HIT for $\mathrm{Re}_\lambda = 100$; — (*Skew.*), ▲ (*Adv.*), ♦ (*Div.*), □ (4S1E), ○ (3S2E). (a) Time evolution of kinetic energy normalized by the steady-state value. Time is expressed in a viscous scale. (b) Three-dimensional energy spectra at $t^* = 330$. Energy is normalized by the steady-state value. Dashed line: DNS.

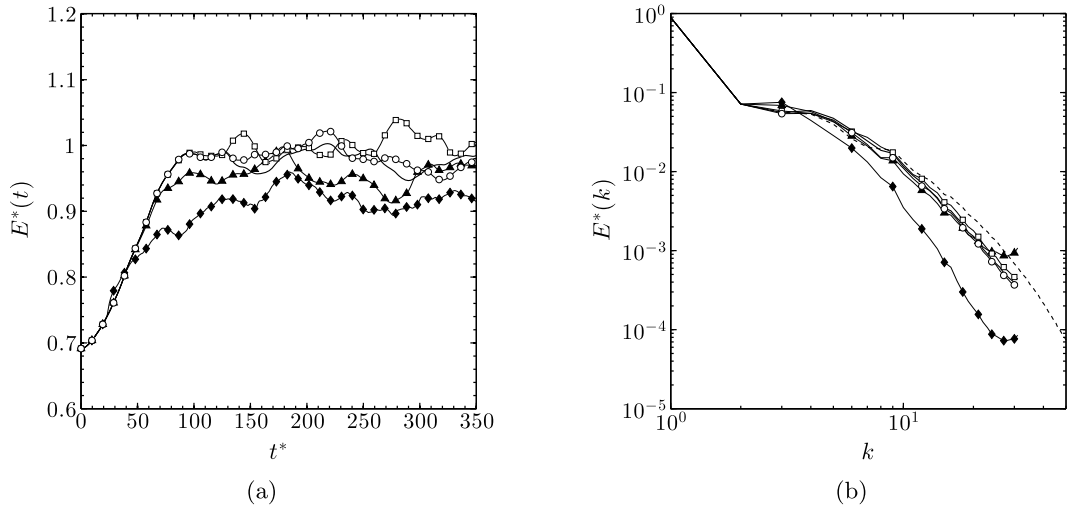


**Fig. 7.** Results for large-eddy simulation of forced HIT for $\mathrm{Re}_\lambda = 170$; — (*Skew.*), ▲ (*Adv.*), ♦ (*Div.*), □ (4S1E), ○ (3S2E). (a) Time evolution of kinetic energy normalized by the steady-state value. Time is expressed in a viscous scale. (b) Three-dimensional energy spectra at $t^* = 330$. Energy is normalized by the steady-state value. Dashed line: DNS.

are suitably alternated within the stages to retain the conservation properties of the skew-symmetric form up to a certain order of accuracy. A comprehensive theoretical framework has been established to derive new alternating Runge–Kutta methods with prescribed order of accuracy on both solution and energy conservation. Direct and large-eddy simulations of homogeneous isotropic turbulence have proved that, in practical situations, these new methods provide results consistent with those of standard skew-symmetric schemes, while halving the computational effort required for the evaluation of the convective term. The advantage in terms of the global CPU time depends upon the details of the algorithm. In general, the new schemes are highly convenient is situations where the computation of the nonlinear term takes a large part of the overall CPU time. For instance, in a periodic, fully-spectral framework, the Poisson equation as well as the viscous terms need a negligible computational effort, and the time-saving proved to reach up to 43% of the total time. The method is then very suitable for spectral codes for direct numerical simulations of homogeneous isotropic turbulence. In particular, the 3S2E(4) scheme, i.e., third-order accurate on solution and second-order accurate on energy-conservation, yielded remarkably good results, and is thus recommended to be used in place of the more costly skew-symmetric form. The 4S1E(4) scheme, despite showing in some cases slightly inferior performances, has also demonstrated an acceptable robustness and can be conveniently implemented as an alternate version of the commonly used RK4. When a dynamic subgrid-scale model was applied, the total saving dropped to 15%. The SGS model computational cost would be less important for numerical algorithms working in finite-difference or finite-volume contexts, although in this case the projection method has a more

significant impact on the overall CPU time. A notable decrease in the time saving offered by the method would also occur in cases in which some of the extra derivatives of the velocity needed to compute the skew-symmetric form have to be already calculated for other terms (e.g., for the viscous term in a problem including heat transfer with variable viscosity).

A promising extension of the method would be the application of the underlying idea to situations with at least one direction of non-homogeneity, e.g. a channel flow. Discretizations that satisfy a discrete summation-by-parts rule [34] could be coupled to the alternating paradigm proposed here, leading to a significant gain in computational efficiency.

**Acknowledgements**

Part of this work was carried out during the Summer Program 2014 of the Center for Turbulence Research (CTR) at Stanford. The authors are grateful to Prof. Parviz Moin for fruitful discussions during the program, and to Jane Bae for performing preliminary simulations of homogeneous isotropic turbulence with the alternating procedure.

## Appendix A. Solution of nonlinear systems

The four-stage, 3S2E(4) schemes admit solutions only for the two couples of sequences ADAD/DADA and ADDA/DAAD. The nonlinear systems have all four equations in common, which correspond to the third-order conditions for a four-stage method,

$$\begin{aligned}
&b_1+b_2+b_3+b_4=1,\\
&b_2a_{21}+b_3(a_{31}+a_{32})+b_4(a_{41}+a_{42}+a_{43})=\frac{1}{2},\\
&b_2a_{21}^2+b_3(a_{31}+a_{32})^2+b_4(a_{41}+a_{42}+a_{43})^2=\frac{1}{3},\\
&a_{21}(b_3a_{32}+b_4a_{42})+b_4a_{43}(a_{31}+a_{32})=\frac{1}{6}.
\end{aligned} \tag{A.1}$$

These equations have to be augmented by one linear constraint and three nonlinear equations to have second-order accuracy on energy conservation. The form of these equations depends on the specific sequence under study. In particular, for the couple of sequences ADAD/DADA one has, respectively,

$$\begin{aligned}
&b_1-b_2+b_3-b_4=0, && \text{1st order on energy}\\
&\left.\begin{aligned}
&2a_{31}b_3-2a_{32}b_3+4a_{42}b_4-2\,(b_1+b_3)\,(b_1+b_4)=0\\
&(b_2+b_4)^2-2a_{32}b_3=0\\
&(b_1+b_3)^2+2a_{31}b_3-4a_{21}b_2-4a_{41}b_4-4a_{43}b_4=0
\end{aligned}\right\} && \text{2nd order on energy}
\end{aligned} \tag{A.2}$$

and

$$\begin{aligned}
&b_1-b_2+b_3-b_4=0, && \text{1st order on energy}\\
&\left.\begin{aligned}
&4a_{31}b_3-2a_{21}b_2-2b_4\,(a_{41}+2a_{42}-2a_{43})-2\,(b_1+b_3)\,(b_1+b_4)=0\\
&(b_2+b_4)^2+2a_{42}b_4-4a_{32}b_3=0\\
&(b_1+b_3)^2-2a_{21}b_2-2a_{41}b_4-2a_{43}b_4=0
\end{aligned}\right\} && \text{2nd order on energy}
\end{aligned} \tag{A.3}$$

The two systems provide two identical families of solutions, each with two free parameters, which can be expressed in closed-form by the following Butcher array

$$\begin{array}{c|cccc}
0 & & & & \\
\frac{3\theta_1\pm\mathcal{A}}{6\theta_1} & 0 & & & \\
\frac{1}{8\theta_1} & \frac{1}{8\theta_1} & 0 & & \\
-\frac{3\theta_1-16\theta_1\theta_2+4\theta_2\mathcal{B}+4\theta_1\mathcal{B}\pm2\mathcal{A}}{24\theta_1\theta_2} & \frac{1}{8\theta_2} & \frac{\theta_1\pm\mathcal{A}}{6\theta_2} & 0 \\
\hline
\frac{1}{2}-\theta_1 & \frac{1}{2}-\theta_2 & \theta_1 & \theta_2
\end{array},$$

where

$$\mathcal{A}=3\theta_2\sqrt{-\frac{\theta_1(10\theta_1-3)}{3\theta_2(2\theta_2-1)}}, \qquad \mathcal{B}=\theta_1\pm\mathcal{A}.$$

The system admits solutions for

$$\begin{cases}\theta_1\in\,]-\infty,0[\;\cup\;[3/10,+\infty[\\ \theta_2\in\,]0,1/2[\end{cases}\quad\cup\quad\begin{cases}\theta_1\in\,]0,3/10]\\ \theta_2\in\,]-\infty,0[\;\cup\;]1/2,+\infty[.\end{cases} \tag{A.4}$$

In this range, the parameters $\theta_1$ and $\theta_2$ can be optimized to achieve various goals, e.g., low-dissipation and low-dispersion characteristics [35], improved accuracy on pressure [36] or a computationally efficient implementation. For the latter case, a

convenient choice is $\theta_1 = 3/10$ and $\theta_2 = 7/20$, which leads to the Butcher array given in Section 4. However, these families of schemes have a limited stability range, see Appendix B.

The sequences ADDA/DAAD lead to the following conditions:

$$\left.\begin{array}{l} b_1 - b_2 - b_3 + b_4 = 0, \\ 4a_{32}b_3 + 2a_{41}b_4 - 2a_{42}b_4 - 2a_{43}b_4 - 2\,(b_1 + b_4)\,(b_2 + b_3) = 0 \\ (b_2 + b_3)^2 - 2a_{42}b_4 - 2a_{43}b_4 = 0 \\ (b_1 + b_4)^2 + 2a_{41}b_4 - 4a_{21}b_2 - 4a_{31}b_3 = 0 \end{array}\right\} \begin{array}{l} \text{1st order on energy} \\ \\ \text{2nd order on energy} \end{array} \tag{A.5}$$

and

$$\left.\begin{array}{l} b_1 - b_2 - b_3 + b_4 = 0, \\ 2a_{32}b_3 - 2a_{31}b_3 - 2a_{21}b_2 + 4a_{41}b_4 - 2\,(b_1 + b_4)\,(b_2 + b_3) = 0 \\ (b_1 + b_4)^2 - 2a_{21}b_2 - 2a_{31}b_3 = 0 \\ (b_2 + b_3)^2 + 2a_{32}b_3 - 4a_{42}b_4 - 4a_{43}b_4 = 0 \end{array}\right\} \begin{array}{l} \text{1st order on energy} \\ \\ \text{2nd order on energy} \end{array} \tag{A.6}$$

In order to solve the systems, it turns out to be convenient to add two conditions on some coefficients to set them to zero. For instance, adding such conditions on $a_{31}$ and $a_{42}$, it is easy to derive the Butcher array reported in Section 4.

## Appendix B. Stability of new Runge–Kutta schemes

The absolute stability of the newly derived Runge–Kutta schemes can be studied in a classical way by evaluating the so-called *stability function* [25,37]. The latter is derived by applying an RK scheme to a linear differential equation $u'(t) = \lambda u(t)$. For $s$-stage, $s$-order standard Runge–Kutta methods, the stability function is easily proved to be a polynomial of degree $s$ of the type

$$R(\sigma) = 1 + \sigma + \frac{\sigma^2}{2!} + \cdots + \frac{\sigma^s}{s!}, \tag{B.1}$$

where $\sigma = \lambda \Delta t$. If the Butcher array is indicated concisely as

$$\begin{array}{c|c} \mathbf{c} & \mathbf{A} \\ \hline & \mathbf{b}^T \end{array},$$

then the stability function is given by

$$R(\sigma) = 1 + \sigma \mathbf{b}^T \left(\mathbf{I} - \sigma \mathbf{A}\right)^{-1} \mathbf{1}^T. \tag{B.2}$$

Equation (B.2) can be used to calculate the stability function of the newly derived Runge–Kutta schemes given in Appendix A. In particular, one of the two-parameter families of ADAD/DADA-3S2E(4) schemes has the stability function

$$\begin{aligned} R(\sigma) = 1 + \sigma &+ \left(\frac{1}{2} - \frac{\sqrt{3}\theta_2 \mathcal{A}}{9\theta_1}\right)\sigma^2 + \left(\frac{1}{6} + \frac{\sqrt{3}\mathcal{A}}{36\theta_1}\right)\sigma^3 \\ &+ \left(\frac{\sqrt{3}\mathcal{A}}{216\theta_1} - \frac{15\theta_1 - 9/2}{\theta_1\,(576\theta_2 - 288)} - \frac{24\theta_1 - 9}{576\theta_1}\right)\sigma^4. \end{aligned} \tag{B.3}$$

A term-to-term comparison between Eq. (B.1) and Eq. (B.3) shows that in order to match the low-order coefficients, it must result $\mathcal{A} = 0$, hence $\theta_1 = 3/10$. However, this choice leads to a violation of the fourth-order coefficient. The same result is obtained with the other two-parameter family. As a consequence, the ADAD/DADA − 3S2E(4) schemes cannot be fourth-order accurate for linear equations, and therefore have the linear stability footprint of a three-stage, third-order scheme.

On the contrary, by applying Eq. (B.2) to the Butcher array resulting from ADDA/DAAD − 3S2E(4) schemes, and reported in Section 4.2, it can be found that it has the stability function of a four-stage, fourth-order scheme, and hence the same stability region. It is thus to be preferred to ADAD/DADA schemes.

## References

[1] R. Mittal, P. Moin, Suitability of upwind-biased finite difference schemes for large-eddy simulation of turbulent flows, J. Comput. Phys. 35 (1997) 1415–1417.
[2] N.A. Phillips, An example of nonlinear computational instability, in: The Atmosphere and the Sea in Motion, Rockefeller Institute Press, Oxford University Press, 1959, pp. 501–504.
[3] B. Koren, R. Abgrall, P. Bochev, J. Frank, B. Perot, Physics-compatible numerical methods, J. Comput. Phys. 257 (2013) 1039.
[4] J.B. Perot, Discrete conservation properties of unstructured mesh schemes, Annu. Rev. Fluid Mech. 43 (2011) 299–318.
[5] S. Ghosal, An analysis of numerical errors in large-eddy simulations of turbulence, J. Comput. Phys. 125 (1996) 187–206.
[6] R.W.C.P. Verstappen, A.E.P. Veldman, Symmetry-preserving discretization of turbulent flow, J. Comput. Phys. 187 (2003) 343–368.
[7] Y. Morinishi, T.S. Lund, O.V. Vasilyev, P. Moin, Fully conservative higher order finite difference schemes for incompressible flows, J. Comput. Phys. 143 (1998) 90–124.

[8] G.A. Blaisdell, E.T. Spyropoulos, J.H. Qin, The effect of the formulation of nonlinear terms on aliasing errors in spectral methods, Appl. Numer. Math. 21 (3) (1996) 207–219.
[9] A.G. Kravhcenko, P. Moin, On the effect of numerical errors in large eddy simulations of turbulent flows, J. Comput. Phys. 131 (1997) 310–322.
[10] N.N. Mansour, P. Moin, W.C. Reynolds, J.H. Ferziger, Improved methods for large eddy simulations of turbulence, in: Turbulent Shear Flows 1, 1979, pp. 386–401.
[11] K. Horiuti, Comparison of conservative and rotational forms in large eddy simulation of turbulent channel flow, J. Comput. Phys. 71 (1987) 343–370.
[12] W.J. Feiereisen, W.C. Reynolds, J.H. Ferziger, Numerical simulation of compressible, homogeneous turbulent shear flow, Tech. rep., Stanford University.
[13] Y. Morinishi, Skew-symmetric form of convective terms and fully conservative finite difference schemes for variable density low-Mach number flows, J. Comput. Phys. 229 (2010) 276–300.
[14] A.E. Honein, P. Moin, Higher entropy conservation and numerical stability of compressible turbulence simulations, J. Comput. Phys. 201 (2004) 531–545.
[15] S. Pirozzoli, Generalized conservative approximations of split convective derivative operators, J. Comput. Phys. 229 (19) (2010) 7180–7190.
[16] F. Ducros, F. Laporte, T. Soulères, V. Guinot, P. Moinat, B. Caruelle, High-order fluxes for conservative skew-symmetric-like schemes in structured meshes: application to compressible flows, J. Comput. Phys. 161 (2000) 114–139.
[17] J.C. Kok, A high-order low-dispersion symmetry-preserving finite-volume method for compressible flow on curvilinear grids, J. Comput. Phys. 228 (2009) 6811–6832.
[18] S. Laizet, E. Lamballais, High-order compact schemes for incompressible flows: a simple and efficient method with quasi-spectral accuracy, J. Comput. Phys. 228 (2009) 5989–6015.
[19] W. Cheng, R. Samtaney, A high-resolution code for large eddy simulation of incompressible turbulent boundary layer flows, Comput. Fluids 92 (2014) 82–92.
[20] J.F. Gibson, Channelflow: a spectral Navier–Stokes simulator in C++, Tech. rep., U. New Hampshire, 2014, http://Channelflow.org.
[21] G.E. Karniadakis, S. Sherwin, Spectral/hp Element Methods for Computational Fluid Dynamics, Oxford University Press, 2005.
[22] T.A. Zang, On the rotation and skew-symmetric forms for incompressible flow simulations, Appl. Numer. Math. 7 (1991) 27–40.
[23] B. Sanderse, Energy-conserving Runge–Kutta methods for the incompressible Navier–Stokes equations, J. Comput. Phys. 233 (2013) 100–131.
[24] F. Capuano, G. Coppola, L. de Luca, An efficient time advancing strategy for energy-preserving simulations, J. Comput. Phys. 295 (2015) 209–229.
[25] J.C. Butcher, Numerical Methods for Ordinary Differential Equations, Wiley, 2004.
[26] S.K. Lele, Compact finite difference schemes with spectral-like resolution, J. Comput. Phys. 103 (1992) 16–42.
[27] H.A. van der Vorst, BI-CGSTAB: a fast and smoothly converging variant of BI-CG for the solution of nonsymmetric linear systems, SIAM J. Sci. Stat. Comput. 13 (1992) 631–644.
[28] H.K.B. Vreman, B. Geurts, Comparison of numerical schemes in large-eddy simulation of the temporal mixing layer, Int. J. Numer. Methods Fluids 22 (1996) 297–311.
[29] H. Le, P. Moin, An improvement of fractional step methods for the incompressible Navier–Stokes equations, J. Comput. Phys. 92 (1991) 369–379.
[30] J.-B. Lagaert, G. Balarac, G.-H. Cottet, Hybrid spectral-particle method for the turbulent transport of a passive scalar, J. Comput. Phys. 260 (2014) 127–142.
[31] E.D. Siggia, G.S. Patterson, Intermittency effects in a numerical simulation of stationary three-dimensional turbulence, J. Fluid Mech. 86 (1978) 567–592.
[32] M. Germano, U. Piomelli, P. Moin, W.H. Cabot, A dynamic subgrid-scale eddy viscosity model, Phys. Fluids A 3 (1991) 1760–1765.
[33] D. Lilly, A proposed modification of the Germano subgrid-scale closure method, Phys. Fluids A 4 (1992) 633–635.
[34] M. Svard, J. Nordstrom, Review of summation-by-parts schemes for initial-boundary-value problems, J. Comput. Phys. 268 (2014) 17–38.
[35] F.Q. Hu, M.Y. Hussaini, J.L. Manthey, Low-dissipation and low-dispersion Runge–Kutta schemes for computational acoustics, J. Comput. Phys. 124 (1996) 177–191.
[36] B. Sanderse, B. Koren, Accuracy analysis of explicit Runge–Kutta methods applied to the incompressible Navier–Stokes equations, J. Comput. Phys. 231 (2012) 3041–3063.
[37] D.F. Griffiths, D.J. Higham, Numerical Methods for Ordinary Differential Equations, Springer, 2010.